

QCD at non-zero density and canonical partition functions with Wilson fermions

Andrei Alexandru^a and Urs Wenger^b

^a Physics Department, The George Washington University
Washington, DC 20052, USA

^b Albert Einstein Center for Fundamental Physics
Institute for Theoretical Physics, Sidlerstrasse 5, CH-3012 Bern, Switzerland

Abstract

We present a reduction method for Wilson Dirac fermions with non-zero chemical potential which generates a dimensionally reduced fermion matrix. The size of the reduced fermion matrix is independent of the temporal lattice extent and the dependence on the chemical potential is factored out. As a consequence the reduced matrix allows a simple evaluation of the Wilson fermion determinant for any value of the chemical potential and hence the exact projection to the canonical partition functions.

1 Introduction

Non-perturbative lattice calculations of Quantum Chromodynamics (QCD) at zero density have seen remarkable progress in recent years. However, simulations at non-zero quark or baryon density remain a challenge due to the occurrence of a complex phase in the fermion determinant at non-zero chemical potential. The fluctuation of this phase is the source of the notorious fermionic sign problem and obstructs the straightforward simulation of the theory using Monte-Carlo importance sampling. This problem limits the reliability of present day lattice QCD calculations at finite baryon density and makes it difficult to explore the QCD phase diagram in parameter regimes which are particularly interesting, e.g. for the identification of different phases of matter, the determination of phase transition lines and the location of possible critical endpoints. However, credible non-perturbative results at non-zero quark density would provide important phenomenological information, e.g. for understanding the structure of neutron stars or the dynamics of relativistic heavy-ion collisions.

One approach to QCD at finite density makes use of the canonical formulation where the net quark (or baryon) number is held constant. This can be achieved by separating the grand-canonical partition function Z_{GC} into a sum of canonical partition functions $Z_C(k)$ with a fixed net number k of quarks and anti-quarks. Quantities at fixed chemical potential, i.e. in the standard grand-canonical formulation of QCD, can then be obtained by averaging over the canonical partition functions. It turns out that the projection to the canonical sectors can

be done exactly, gauge field by gauge field, however it requires the integration of the fermion determinant over the whole range of imaginary chemical potential $\phi = i\mu/T \in [0, 2\pi]$.

In the past this approach could only be made practical in connection with staggered fermions. For those, clever fermion matrix reduction methods were developed [1, 2, 3] that allow the evaluation of the determinant for any value of the chemical potential once the eigenvalues of the reduced fermion matrix are known. In this approach the reduction of the fermion matrix in size by a factor half the temporal lattice extent is the crucial ingredient since it reduces the complexity of the eigenvalue computation by the corresponding factor cubed. Unfortunately, however, for Wilson fermions so far no such reduction method was known despite various attempts [4, 5].

In this paper we present such a reduction method for Wilson fermions, i.e. we derive a dimensionally reduced Wilson fermion matrix whose size is independent of the temporal lattice extent and for which the dependence on the chemical potential is factored out. It therefore allows easy and exact evaluation of the determinants at any value of the chemical potential and hence the straightforward projection to the various canonical sectors. Applications which are facilitated by the reduction method for Wilson fermions presented here include the reweighting of ensembles to different values of the chemical potential and calculations based on canonical ensembles [6, 7, 8, 9].

The reduction of the four dimensional Wilson Dirac operator to the three dimensional reduced fermion matrix is very similar to the construction of the four dimensional overlap operator from the five dimensional domain wall fermion operator [10, 11, 12]. A similar reduction method for the Wilson fermion matrix has also been proposed in [13] in the context of reweighting with stochastic determinants. Finally, while preparing the paper we were informed by Nakamura and Nagata [14] about their development of similar reduction techniques for the Wilson fermion matrix.

The paper is organized as follows. In section 2 we briefly review the separation of the grand-canonical partition function of QCD into a sum of canonical partition functions with fixed quark or baryon number. In section 3 we present the reduction method for Wilson fermions which renders the computational complexity of the determinant independent of the temporal lattice extent and factorizes the dependence on the chemical potential. In section 4 and 5 we discuss spectral properties of the reduced matrix and some properties of the projected determinants, respectively. While the results from these sections so far do not have a direct physical application, we would like to emphasise their potential importance for the development of new canonical simulation algorithms, or for the optimization of reweighting strategies. Finally, in section 6 we present some results from a reweighting of canonical ensembles, merely as a demonstration of the potential of the reduced fermion matrix approach.

2 Canonical formulation of QCD at fixed baryon number

The grand-canonical partition function at temperature T and chemical potential μ_q for a single quark flavor can be defined as

$$Z_{GC}(\mu_q) = \int \mathcal{D}U e^{-S_g(U)} \det M(U, \mu_q), \quad (1)$$

where $M(U, \mu_q)$ denotes the Dirac operator, U collects the gauge field degrees of freedom from the color gauge group $SU(N_c)$ and $S_g(U)$ is the gauge field action. This is the commonly used partition function for simulating QCD thermodynamics on the lattice [15, 16, 17, 18], which in general, however, suffers from a strong fermionic sign problem. The same thermodynamic physics can also be extracted using the canonical partition function [6, 7, 19, 20, 21], although one should keep in mind that the physics of the two systems strictly coincide only in the thermodynamic limit, i.e. in the limit of infinite spatial volume. The partition function in the canonical approach, for a system with a net number of k quarks, can be written as

$$Z_C(k) = \int \mathcal{D}U e^{-S_g(U)} \det_k M(U), \quad (2)$$

where the fermionic contribution is now included in the projected determinant

$$\det_k M(U) \equiv \frac{1}{2\pi} \int_0^{2\pi} d\phi e^{-ik\phi} \det M(U, \mu_q = i\phi T) \quad (3)$$

and one has made use of the fact that $\det M(U, \mu_q = i\phi T)$ enjoys a $\frac{2\pi}{N_c}$ -periodicity in ϕ [22, 23]. The periodicity stems from the fact that a shift in the imaginary chemical potential $\phi \rightarrow \phi + \frac{2\pi}{N_c}$ can be exactly compensated by a corresponding $\mathbb{Z}(N_c)$ -transformation of the underlying gauge field. From this periodicity it also follows that $Z_C(k) = 0$ for $k \neq 0 \pmod{N_c}$, i.e. it vanishes for non-integer baryon numbers $n_B \notin \mathbb{Z}$, while $Z_C(k) = Z_C^*(-k)$ follows from the evenness $Z_{GC}(\mu_q) = Z_{GC}(-\mu_q)$ due to time-reversal symmetry.

Finally, one can relate the canonical partition functions back to the grand-canonical ones using the fugacity expansion

$$Z_{GC}(\mu_q) = \sum_{k=-\infty}^{+\infty} e^{k\mu_q/T} Z_C(k), \quad (4)$$

where the sum can in principle be restricted to $k = 0 \pmod{N_c}$, i.e. integer baryon numbers, following the discussion above. Furthermore, the equation also motivates the determination of the baryon chemical potential in the canonical approach by a definition based on the free energy. Essentially, the baryon chemical potential is the response of the system when introducing one more baryon to the system, i.e.

$$\mu_B(n_B) \equiv F(N_c \cdot (n_B + 1)) - F(N_c \cdot n_B), \quad (5)$$

where $F(k) = -T \log Z_C(k)$ is the Helmholtz free energy of the canonical partition function. In a finite volume V , this definition is ambiguous due to the discreteness of the baryon number, however, in the thermodynamic limit it yields $\mu_B(\rho_B) = df/d\rho_B$, where $\rho_B = n_B/V$ and $f = F/V$ are the baryon and free energy densities. Note that the baryon chemical potential μ_B is different from the quark chemical potential μ_q used above. The quark chemical potential cannot be defined as the increase of the free energy when introducing a quark in the system since the free energy is infinite for systems that have fractional baryon numbers. If we need to compare the chemical potential used in the grand-canonical approach to the chemical potential measured in the canonical approach, we use $\mu_q \simeq \mu_B/N_c$.

3 Reduction technique for the Wilson fermion matrix

In the following we consider QCD with Wilson fermions on a periodic lattice with temporal and spatial extent L_t and L_s , respectively. The quark chemical potential is $\mu \equiv a\mu_q$ where a is the lattice spacing.¹ The massive Wilson-Dirac operator can be written as

$$M = \frac{1}{2}\Gamma_\nu(\nabla_\nu + \nabla_\nu^*) - \frac{1}{2}\nabla_\nu^*\nabla_\nu + m, \quad (6)$$

where ∇_ν, ∇_ν^* denote the covariant forward and backward lattice derivative, Γ_ν are the Euclidean Dirac matrices and m is the bare quark mass. The chemical potential μ couples to the fermion number operator and is introduced on the lattice [24] by furnishing the forward and backward temporal hopping terms by factors of $e^{\pm\mu}$, respectively. More explicitly we have

$$M_{x,y} = (m+4) \cdot \delta_{x,y} - \sum_{k=1}^3 \left\{ P(+k) U_k(x) \delta_{y,x+\hat{k}} + P(-k) U_k^\dagger(y) \delta_{y,x-\hat{k}} \right\} \\ - \left\{ e^{+\mu} P(+4) U_4(x) \delta_{y,x+\hat{4}} + e^{-\mu} P(-4) U_4^\dagger(y) \delta_{y,x-\hat{4}} \right\}, \quad (7)$$

where $U_\nu(x) \in \text{SU}(N_c)$ are the gauge field links and $P(\pm\nu) = \frac{1}{2}(1 \mp \Gamma_\nu)$, $\nu = 1, \dots, 4$. Further, for convenience we introduce $P_\pm \equiv P(\pm 4)$ for the projectors in temporal direction and will use this notation in the following. Choosing the spatial Euclidean Dirac matrices as

$$\Gamma_k = \begin{pmatrix} 0 & \sigma_k \\ \sigma_k^\dagger & 0 \end{pmatrix} \quad (8)$$

and hence hermitian, we note that the spatial part of the Wilson Dirac operator, i.e. the first line of eq.(7), can be written in the form

$$B = \begin{pmatrix} B_{++} & C \\ -C^\dagger & B_{--} \end{pmatrix} \quad (9)$$

where $B_{++} = B_{--}$ is hermitian and trivial in Dirac space,

$$(B_{++})_{x,y} = (m+4) \cdot \delta_{x,y} - \frac{1}{2} \sum_{k=1}^3 \left\{ \delta_{y,x+\hat{k}} U_k(x) + \delta_{x,y+\hat{k}} U_k^\dagger(y) \right\}, \quad (10)$$

while

$$C_{x,y} = \frac{1}{2} \sum_{k=1}^3 \sigma_k \left\{ \delta_{y,x+\hat{k}} U_k(x) - \delta_{x,y+\hat{k}} U_k^\dagger(y) \right\} \quad (11)$$

is hermitian if the Heisenberg matrices σ_k in eq.(8) are chosen to be hermitian. The derivations presented below focus on the un-improved version of the Wilson Dirac operator. However, the addition of the clover term can be easily accommodated: it only changes the spatial hopping matrix B in a way that is consistent with the structure in eq.(9) which is all that is needed for some of the more specific derivations in sections 3.2 and 4.1. In fact, the numerical experiments presented later in the paper use the clover improved version of the Dirac operator.

¹From now on we set $a=1$.

3.1 Reduction of $\det M$

The Wilson fermion matrix (6) in temporal gauge with (anti-)periodic boundary conditions in space (time)direction for a single quark flavor with chemical potential μ can be represented by

$$M = \begin{pmatrix} B_0 & P_+ & & -P_- \cdot \mathcal{U}^\dagger \cdot e^{-\mu L_t} \\ P_- & B_1 & P_+ & \\ & P_- & B_2 & \ddots \\ & & \ddots & \ddots \\ -P_+ \cdot \mathcal{U} \cdot e^{+\mu L_t} & & P_- & B_{L_t-1} \end{pmatrix} \quad (12)$$

where the B_t 's are $(4 \cdot N_c \cdot L_s \times 4 \cdot N_c \cdot L_s)$ -matrices and represent the (spatial) Wilson Dirac operator on time-slice t and where we have rescaled the fermion fields such that the dependence on the chemical potential resides on the links connecting the last and the first time slice. The temporal gauge links also reside only on those links and are collected in the matrix \mathcal{U} so that $P_+ \cdot \mathcal{U}$ is of the same size as B_t . For convenience we abbreviate in the following $A^- \equiv -\mathcal{U}^\dagger \cdot e^{-\mu L_t}$ and $A^+ \equiv -\mathcal{U} \cdot e^{+\mu L_t}$ and note that the matrix can be written in the form

$$M = \begin{pmatrix} B_0 & & & A^- \\ 1 & B_1 & & \\ & \ddots & \ddots & \\ & & 1 & B_{L_t-1} \end{pmatrix} P_- + \begin{pmatrix} B_0 & 1 & & \\ & B_1 & \ddots & \\ & & \ddots & 1 \\ A^+ & & & B_{L_t-1} \end{pmatrix} P_+ \quad (13)$$

using the fact that $P_+ + P_- = 1$. Essentially, this splits the matrix into two parts describing the components of the Dirac particle moving forward and backward in time. Next we define the shift-projection matrix

$$\mathcal{P} = \begin{pmatrix} P_+ & P_- & & \\ & P_+ & P_- & \\ & & P_+ & \ddots \\ & & & \ddots & P_- \\ P_- & & & & P_+ \end{pmatrix} \quad (14)$$

which leaves the forward moving part invariant and shifts the backward moving part by one time slice. We further note that $\det \mathcal{P} = 1$. Multiplying M with \mathcal{P} from the right we find

$$M \cdot \mathcal{P} = \begin{pmatrix} Q_0^-(P_- A^- + P_+) & Q_0^+ & & & \\ & Q_1^- & Q_1^+ & & \\ & & Q_2^- & \ddots & \\ & & & \ddots & Q_{L_t-2}^+ \\ Q_{L_t-1}^+(P_+ A^+ + P_-) & & & & Q_{L_t-1}^- \end{pmatrix} \quad (15)$$

where we defined

$$Q_i^\pm = B_i P_\mp + P_\pm \quad (16)$$

and used the fact that

$$P_- A^- + B_0 P_+ = Q_0^- (P_- A^- + P_+), \quad (17)$$

$$P_+ A^+ + B_{L_t-1} P_- = Q_{L_t-1}^+ (P_+ A^+ + P_-). \quad (18)$$

Now we define the block diagonal matrix

$$\mathcal{Q} = \begin{pmatrix} Q_0^- & & & \\ & Q_1^- & & \\ & & \ddots & \\ & & & Q_{L_t-1}^- \end{pmatrix} \quad (19)$$

and find

$$\tilde{M} \equiv \mathcal{Q}^{-1} \cdot M \cdot \mathcal{P} = \begin{pmatrix} (P_- A^- + P_+) & T_0 & & & \\ & 1 & T_1 & & \\ & & 1 & \ddots & \\ & & & \ddots & T_{L_t-2} \\ T_{L_t-1} (P_+ A^+ + P_-) & & & & 1 \end{pmatrix} \quad (20)$$

where

$$T_i = (Q_i^-)^{-1} \cdot Q_i^+. \quad (21)$$

Note that the matrix \tilde{M} is essentially a transfer matrix describing fermions hopping forward and backward between time slices. We discuss this further in section 3.3.

We can now easily calculate the determinant of the transfer matrix \tilde{M} using Schur complement techniques [12]. Defining

$$T \equiv T_0 \cdot T_1 \cdot \dots \cdot T_{L_t-1} \quad (22)$$

we find

$$\det [\mathcal{Q}^{-1} \cdot M \cdot \mathcal{P}] = \det [(P_- A^- + P_+) - (-1)^{L_t} T \cdot (P_+ A^+ + P_-)] \quad (23)$$

and hence

$$\det [M] = \left(\prod_{i=0}^{L_t-1} \det Q_i^- \right) \cdot \det [\mathcal{Q}^{-1} \cdot M \cdot \mathcal{P}]. \quad (24)$$

Note that the first factor $\det[\mathcal{Q}]$ from canceling the effect of multiplication with \mathcal{Q}^{-1} is independent of μ and cancels when we take the ratio of two determinants, e.g. with two different chemical potentials. Furthermore, from now on we assume L_t to be even in order to get rid of the inconvenient factor $(-1)^{L_t}$.

In order to separate the dependence on the chemical potential μ from the gauge field dependence we first note that for arbitrary matrices A, B, C, D diagonal in Dirac space, i.e. commuting with P_{\pm} , we have

$$(P_{\pm} A + P_{\mp} B)(P_{\pm} C + P_{\mp} D) = P_{\pm} AC + P_{\mp} BD. \quad (25)$$

So multiplying eq.(23) by $\det[P_+ A + P_- B]$ with $A = e^{-\mu L_t}$ and $B = -\mathcal{U}$ we obtain

$$\det [\mathcal{Q}^{-1} \cdot M \cdot \mathcal{P}] \det [P_+ e^{-\mu L_t} - P_- \mathcal{U}] = \det [e^{-\mu L_t} + T \cdot \mathcal{U}]. \quad (26)$$

This is the determinant of the reduced Wilson fermion matrix. Note that the gauge field dependence resides in $T \cdot \mathcal{U}$ only and is completely separated from the dependence on μ . This allows now for an efficient calculation of the determinant as a function of μ for a fixed gauge field background. Denoting the eigenvalues of $T \cdot \mathcal{U}$ by $\lambda_i, i = 1, \dots, 4N_c L_s^3$ we have

$$\det [e^{-\mu L_t} + T \cdot \mathcal{U}] = \prod_{i=1}^{4N_c L_s^3} (e^{-\mu L_t} + \lambda_i). \quad (27)$$

In order to establish the equivalence between $\det[M]$ and eq.(27) we need to cancel the contribution from multiplying with $\det[P_+ e^{-\mu L_t} - P_- \mathcal{U}]$. First we note that the matrix has an inverse,

$$(P_+ e^{+\mu L_t} - P_- \mathcal{U}^\dagger) \cdot (P_+ e^{-\mu L_t} - P_- \mathcal{U}) = 1, \quad (28)$$

hence the canceling is always possible. In fact we can calculate the determinant explicitly, since the matrix splits into the two orthogonal blocks $\propto P_\pm$ (this is due to the fact that \mathcal{U} and $e^{-\mu L_t}$ are trivial in Dirac space) and the determinant is just the product of the determinants of the two subblocks,

$$\det[P_+ e^{-\mu L_t} - P_- \mathcal{U}] = \det[e^{-\mu L_t}] \cdot \det[-\mathcal{U}] = e^{-\mu L_t \cdot 2N_c L_s^3} \quad (29)$$

where the factor of 2 in the exponent comes from the fact that the subblock matrix spans over only half the Dirac indices.

3.2 Calculation of T

A drawback of the matrix reduction is that we need to explicitly calculate T which contains the inverses of Q_i^- of size $(4N_c L_s^3) \times (4N_c L_s^3)$. It turns out, however, that the size of the matrix to be inverted can be halved. To see this consider the following explicit form of Q_i^- . The spatial Wilson Dirac operator B_i on time slice i inherits the structure of the full spatial Wilson Dirac operator B according to eq.(9). When the σ_k in Γ_k are chosen to be hermitian it can be written as

$$B_i = \begin{pmatrix} D_i & C_i \\ -C_i & D_i \end{pmatrix} \quad (30)$$

with $D_i^\dagger = D_i$ and $C_i^\dagger = C_i$ ². Then, in a basis where Γ_4 is block diagonal, one has

$$Q_i^- = P_- + B_i P_+ = \begin{pmatrix} D_i & 0 \\ -C_i & 1 \end{pmatrix}. \quad (31)$$

We then find for the inverse of Q_i^-

$$(Q_i^-)^{-1} = \begin{pmatrix} D_i^{-1} & 0 \\ C_i \cdot D_i^{-1} & 1 \end{pmatrix}, \quad (32)$$

so B_i needs to be inverted only in the subspace proportional to P_+ , i.e. only D_i^{-1} is needed. Further we also need to calculate $\det[Q_i^-]$ although these factors cancel exactly in the ratio

²Note that a similar argument goes through for the choice of antihermitian Dirac matrices in which case one has $C_i^\dagger = -C_i$.

of determinants, e.g. for different chemical potentials. From eq.(31) we read off $\det[Q_i^-] = \det[D_i]$. Finally, for later use we also note the explicit form of Q_i^+ ,

$$Q_i^+ = P_+ + B_i P_- = \begin{pmatrix} 1 & C_i \\ 0 & D_i \end{pmatrix}. \quad (33)$$

3.3 Physical interpretation of the reduced matrix

It is straightforward to give a physical interpretation of the dimensionally reduced Wilson Dirac fermion matrix. The equivalence of the determinants

$$\det M = \det \mathcal{Q} \cdot \det \left[e^{-\mu L_t/2} + T \cdot \mathcal{U} \cdot e^{+\mu L_t/2} \right] \quad (34)$$

establishes an equivalence (up to the bulk term $\det \mathcal{Q}$) between the four-dimensional Wilson Dirac operator M and the effective three-dimensional operator $e^{-\mu L_t/2} + T \cdot \mathcal{U} \cdot e^{+\mu L_t/2}$, similar to the equivalence between the five-dimensional domain wall fermion operator and the four-dimensional overlap Dirac operator [10, 11, 12]. The analogy becomes even more transparent at $\mu = 0$ when the reduced operator becomes $1 + T \cdot \mathcal{U}$, similar to the massless overlap Dirac operator. The factors $e^{\pm\mu L_t/2}$ can then be understood as mass terms for the fermions and anti-fermions propagating forward and backward in time.

This picture is corroborated by the matrix \tilde{M} in eq.(20) which is essentially a transfer matrix describing fermions and (anti-)fermions hopping forward and backward between time slices, respectively. The dynamics of these hoppings are described by the transfer matrices T_i which, however, are independent of μ . Fermions winding around the time direction in forward direction will eventually pick up a factor $e^{+\mu L_t}$ (residing in A^+) for each winding while the anti-fermions winding around the time direction in backward direction will pick up corresponding factors of $e^{-\mu L_t}$ (residing in A^-). In addition, the winding fermion modes are then weighted by \mathcal{U} which contains the temporal gauge field dynamics. In that sense, the reduced matrix is equivalent to a fermion winding number expansion.

To complement this interpretation it is worthwhile to consider alternative forms of the reduced matrix. In the present form the reduced matrix $e^{-\mu L_t/2} + T \cdot \mathcal{U} \cdot e^{+\mu L_t/2}$ makes the propagation of the fermion forward in time explicit. One can equally well emphasize the propagation of the anti-fermion backwards in time. This can for example be achieved by considering, instead of $\mathcal{Q}^{-1} \cdot M \cdot \mathcal{P}$, the dimensional reduction of $\mathcal{P} \cdot M \cdot \tilde{\mathcal{Q}}^{-1}$ where $\tilde{\mathcal{Q}}$ is the block diagonal matrix containing Q_i^+ along the diagonal. The reduced matrix then becomes

$$e^{+\mu L_t/2} + \mathcal{U}^\dagger \cdot \tilde{T} \cdot e^{-\mu L_t/2} \quad (35)$$

where

$$\tilde{T} = \tilde{T}_{L_t-1} \cdot \dots \cdot \tilde{T}_1 \cdot \tilde{T}_0 \quad \text{with} \quad \tilde{T}_i = T_i^{-1}, \quad (36)$$

so making the backward propagation of the anti-fermions (and their weighting with $-\mu$ instead of $+\mu$) explicit. ³

Finally, the construction of the reduced matrix presented in section 3.1 is done for gauge field configurations fixed to temporal gauge. However, the construction can easily be extended

³We note that further equivalent variants of the reduced matrix can be obtained. By considering projection of M with \mathcal{P}^\dagger instead of \mathcal{P} from the left or right, one is lead to reduced matrices with modified T' or $\tilde{T}' = T'^{-1}$ related to the original T by $T' = \tilde{T}^\dagger$.

to the generic case without gauge fixing, leading to a reduced matrix where the structure $T \cdot \mathcal{U}$ becomes

$$T_0 \cdot \mathcal{U}_0 \cdot T_1 \cdot \mathcal{U}_1 \cdot \dots \cdot T_{L_t-1} \cdot \mathcal{U}_{L_t-1} = \prod_{i=0}^{L_t-1} T_i \cdot \mathcal{U}_i. \quad (37)$$

Here the matrices \mathcal{U}_t now collect all the temporal gauge links at fixed time coordinate t , so the matrix \mathcal{U}_{L_t-1} is just \mathcal{U} from before. The factors in the product of eq.(37) can be cyclically permuted without changing the physical content, i.e. the spectrum of the reduced matrix. This is due to the fact that all the cyclic permutations are related to each other by similarity transformations (involving the matrices \mathcal{U}_i and T_i which have determinant one, cf. section 4.1) while the first term in the reduced matrix is trivial in Dirac and color space.

4 Spectral properties of the reduced matrix

4.1 Symmetry of $T \cdot \mathcal{U}$

In the construction of the reduced Wilson fermion matrix the crucial object is the matrix $T \cdot \mathcal{U}$. It turns out that this matrix has interesting properties which express themselves in peculiar symmetry properties of the eigenvalue spectrum.

The first thing to note is that

$$\det T \cdot \mathcal{U} = 1. \quad (38)$$

This can easily be seen from eq.(32) and eq.(33) where we read off $\det(Q_i^-)^{-1} = \det D_i^{-1}$ and $\det Q_i^+ = \det D_i$, respectively, and hence $\det T_i = \det [(Q_i^-)^{-1} \cdot Q_i^+] = 1$.

Secondly, we note that the eigenvalues of $T \cdot \mathcal{U}$ come in pairs: for every eigenvalue of λ , there is an eigenvalue $\lambda' = 1/\lambda^*$. This can be seen as follows. The product $T_i = (Q_i^-)^{-1} \cdot Q_i^+$ can be LDU-decomposed with the help of eq.(32) and eq.(33):

$$(Q_i^-)^{-1} \cdot Q_i^+ = \begin{pmatrix} 1 & 0 \\ C_i & 1 \end{pmatrix} \begin{pmatrix} D_i^{-1} & 0 \\ 0 & D_i \end{pmatrix} \begin{pmatrix} 1 & C_i \\ 0 & 1 \end{pmatrix}. \quad (39)$$

In this form it is easy to calculate its hermitian conjugated inverse, i.e.

$$\left[((Q_i^-)^{-1} \cdot Q_i^+)^{-1} \right]^\dagger = \begin{pmatrix} 1 & -C_i \\ 0 & 1 \end{pmatrix} \begin{pmatrix} D_i & 0 \\ 0 & D_i^{-1} \end{pmatrix} \begin{pmatrix} 1 & 0 \\ -C_i & 1 \end{pmatrix}. \quad (40)$$

Comparing this with eq.(39) we find that

$$\left[((Q_i^-)^{-1} \cdot Q_i^+)^{-1} \right]^\dagger = S \cdot ((Q_i^-)^{-1} \cdot Q_i^+) \cdot S^{-1} \quad \text{with} \quad S = \begin{pmatrix} 0 & 1 \\ -1 & 0 \end{pmatrix}, \quad (41)$$

and hence

$$\left[(T \cdot \mathcal{U})^{-1} \right]^\dagger = S \cdot (T \cdot \mathcal{U}) \cdot S^{-1}. \quad (42)$$

As a consequence the matrix $T \cdot \mathcal{U}$ shares the eigenvalue spectrum with its hermitian conjugated inverse, that is, for each eigenvalue $\lambda \in \text{spec}(T \cdot \mathcal{U})$ there is another eigenvalue $1/\lambda^* \in \text{spec}(T \cdot \mathcal{U})$. The spectral symmetry hints at the possibility that the reduced matrix could be further compressed in size by a factor of two without losing any spectral information. In principle this can be achieved by the projection of $T \cdot \mathcal{U}$ to a suitable subspace, but so far we have not been able to construct such a projection, essentially due to the fact that $T \cdot \mathcal{U}$ is non-normal.

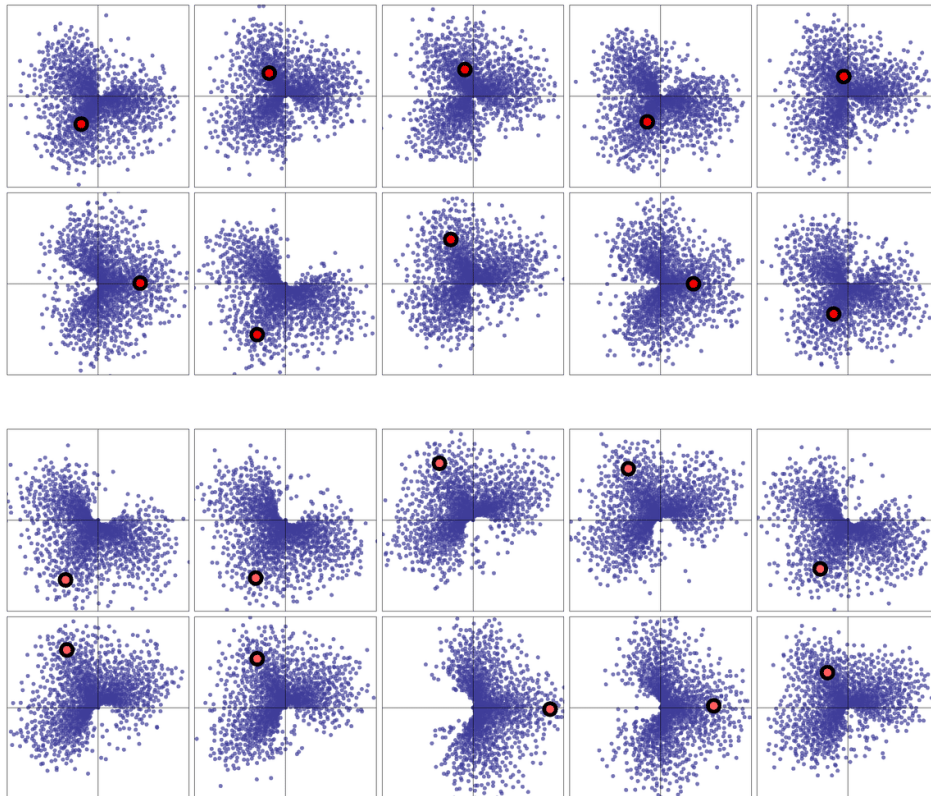


Figure 1: The eigenvalue distribution for 10 arbitrary configurations drawn from canonical ensembles with $n_B = 4$ (top) and $n_B = 11$ (bottom). The red point indicates a scaled value of the spatially averaged Polyakov loop to show its correlation with the eigenvalue distribution.

4.2 Eigenvalue distribution of the reduced matrix

So far we have been concerned with purely algebraic properties of the Wilson Dirac matrix M and the corresponding reduced matrix $T \cdot \mathcal{U}$. In practice, what is needed are all the eigenvalues λ_i of the latter matrix, such that the determinant of $M(\mu)$ can be evaluated for any arbitrary value of the chemical potential according to

$$\det M(\mu) = \det \mathcal{Q} \cdot e^{+\mu L_t \cdot 2N_c L_s^3} \prod_{i=1}^{4N_c L_s^3} (e^{-\mu L_t} + \lambda_i). \quad (43)$$

Apart from the symmetry property $\lambda \leftrightarrow 1/\lambda^*$ discussed in section 4.1 the eigenvalue spectrum has additional interesting features. To illustrate these we will use configurations generated for a previous study of non-zero baryon density systems using the canonical partition function [25]. These $6^3 \times 4$ configurations are picked from $N_f = 4$ ensembles at a temperature close to the deconfining transition: $T \approx 0.95T_c$. The parameters for the fermionic matrix will be set to the values used to generate the ensembles: $\kappa = 0.1371$ and $c_{sw} = 1.96551$ corresponding to a pion mass of about 700 – 800 MeV.

In Fig. 1 we plot the eigenvalue distribution of the matrix $T \cdot \mathcal{U}$ for a random selection of gauge field configurations drawn from canonical ensembles with baryon number $n_B = 4$ (top

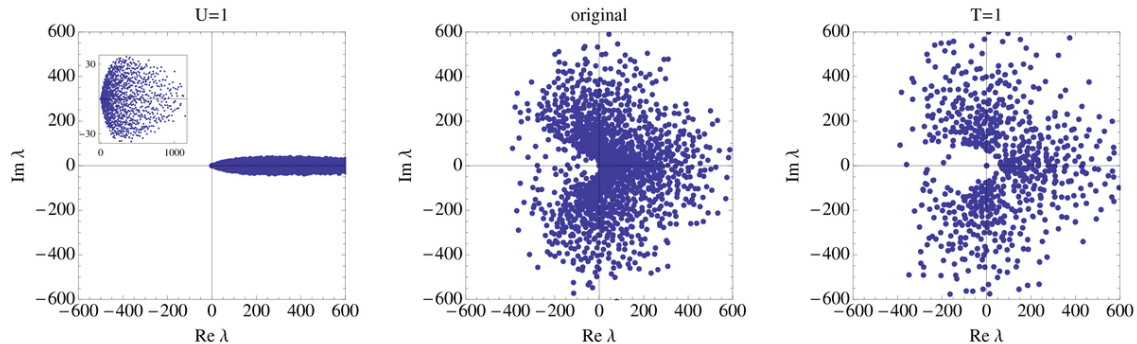


Figure 2: The eigenvalue spectrum of $T \cdot \mathcal{U}$ for an arbitrary configuration with $\arg P(U) \approx 0$ (middle plot), in the case when $\mathcal{U} = 1$ is put by hand (left plot), or when all spatial links are set to one (right plot).

two rows) and $n_B = 11$ (bottom two rows), respectively. The plots represent the eigenvalue distribution in the complex plane and the scale is from $\text{Re}, \text{Im } \lambda \in [-600, 600]$. Only the large magnitude eigenvalues are visible (the low magnitude members are also plotted but they are not visible on this scale). Note that there is a cone empty for each configuration and that the distributions exhibit a three lobe structure which, from configuration to configuration, is related by $\mathbb{Z}(3)$ -rotations in the complex plane. An interesting observation is the fact that for each configuration the structure is correlated with the value of the spatially averaged Polyakov loop, which in the temporal gauge is given by

$$P(U) = \frac{1}{4N_c L_s^3} \text{tr } \mathcal{U}. \quad (44)$$

In Fig. 1 we make this correlation explicit for each configuration by imposing the corresponding (rescaled) value of $P(U)$ onto the eigenvalue spectrum. Of course this correlation is no surprise, since from the structure $T \cdot \mathcal{U}$ it is immediately clear that under a $\mathbb{Z}(3)$ -transformation of the temporal gauge fields \mathcal{U} the eigenvalues are simply rotated by the corresponding $\mathbb{Z}(3)$ factor. On the other hand, one should also keep in mind that some of the correlations we observe between the determinant and the Polyakov loop might be due to the rather heavy quark mass [26] and the correlations might become less pronounced as we move towards lower quark masses.

In order to further expose the influence of the $\mathbb{Z}(3)$ phase of $P(U)$ (or rather \mathcal{U}) on the spectrum, we perform the following exercise. Instead of computing the eigenvalues of the original reduced matrix $T \cdot \mathcal{U}$, we calculate the spectrum of a modified reduced matrix where we set the temporal gauge fields \mathcal{U} to the $\mathbb{Z}(3)$ phase as given by the Polyakov loop $P(U)$. We show the result of this calculation for a configuration with $\arg P(U) \simeq 0$ in Fig. 2 in the left most plot. The only gauge field dependence is now through the spatial gauge links in T and we see that this dependence is responsible for the eigenvalues' variation in magnitude, while the phase of the eigenvalues fluctuates very weakly around zero. (Note that the spectrum of the reduced free Wilson Dirac operator is real and the eigenvalues $\lambda > 1$ span the range between roughly 6 and 2000.) Of course we can also turn the argument around and put all the spatial links to unity, so that the gauge field dependence resides in \mathcal{U} alone. The spectrum of the reduced matrix modified in this way is shown in the right most plot in Fig. 2. Comparing this with the original spectrum shown in the middle plot we conclude that the

phase variation of the eigenvalues is determined almost solely by the temporal gauge fields \mathcal{U} while the spatial gauge fields only add small fluctuations to the phase. In Fig. 11 we repeat this exercise for configurations with $\arg P(U) \simeq \pm 2\pi/3$. As discussed above, in this case the spectra are simply rotated by the corresponding $\mathbb{Z}(3)$ factors, and the conclusion remains the same.

5 Projected determinant of the canonical partition function

After having discussed the properties of the reduced matrix and its spectrum, the next interesting quantity to study is the determinant as a function of the (real or imaginary) chemical potential, and eventually also the projected determinant which subsumes the dynamics of the fermions in the canonical partition function.

5.1 The determinant at non-zero chemical potential

Having the eigenvalues λ_i of $T \cdot \mathcal{U}$ at hand it is now easy to evaluate the determinant of the Wilson Dirac operator for arbitrary chemical potential according to eq.(43). In Fig. 3 we show the logarithm of the determinant $\det M(\mu)$ for three configurations from a canonical ensemble with $n_B = 4$. From top to bottom the configurations have $\arg P(U) \approx 0, +2\pi/3$ and $-2\pi/3$. The first row shows the logarithm of $|\det M(\mu)|$ normalized to $\det M(\mu = 0)$, i.e. $|\log \det M(\mu)| / \det M(\mu = 0)$, while the second row shows the argument $\arg \det M(\mu)$ modulo 2π . We note significant differences between the results for configurations in the various triality sectors. Firstly, while in all sectors the size of the determinant ratio starts to grow exponentially with $|\mu|$ beyond $|\mu| \gtrsim 1$, configurations in the non-trivial $\mathbb{Z}(3)$ -sectors show a local minimum just below $|\mu| \sim 1$ in contrast to configurations in the trivial sector which show a monotonic increase with $|\mu|$. Secondly, the derivative of the phase w.r.t. μ stays roughly constant for $|\mu| \lesssim 0.5$, but depends strongly on the $\mathbb{Z}(3)$ -sector.

In Fig. 4 we show the same kind of plots for three typical configurations (with $\arg P(U) \approx 0, +2\pi/3$ and $-2\pi/3$ from top to bottom) from a canonical ensemble with $n_B = 11$. The picture qualitatively remains the same except that the features described before are accentuated. For configurations in the non-trivial $\mathbb{Z}(3)$ -sectors the minima of $|\det M(\mu)|$ become slightly deeper and move to slightly larger values of $|\mu|$. Furthermore, for those configurations the phase of $\det M(\mu)$ changes more rapidly while the change of the phase in the trivial $\mathbb{Z}(3)$ -sector becomes smoother and stretches further into larger values of $|\mu|$, possibly allowing reweighting to larger chemical potential.

Note that the wild phase fluctuations observed for configurations with non-trivial Polyakov loop are due to the contributions from the fractional baryon number sectors. To illustrate this point, following the ideas presented in [23], we define a modified determinant that only includes the integral baryon number sectors:

$$\det \hat{M}(U, \mu) \equiv \sum_{n_B} e^{3n_B \mu/T} \det_{3n_B} M(U). \quad (45)$$

This definition is equivalent to the fugacity expansion for the determinant where we only sum over the sectors that have a net number of quarks divisible by 3. In figure 5 we plot the absolute value and phase of this modified determinant for a configuration with $\arg P(U) \approx 2\pi/3$ (the

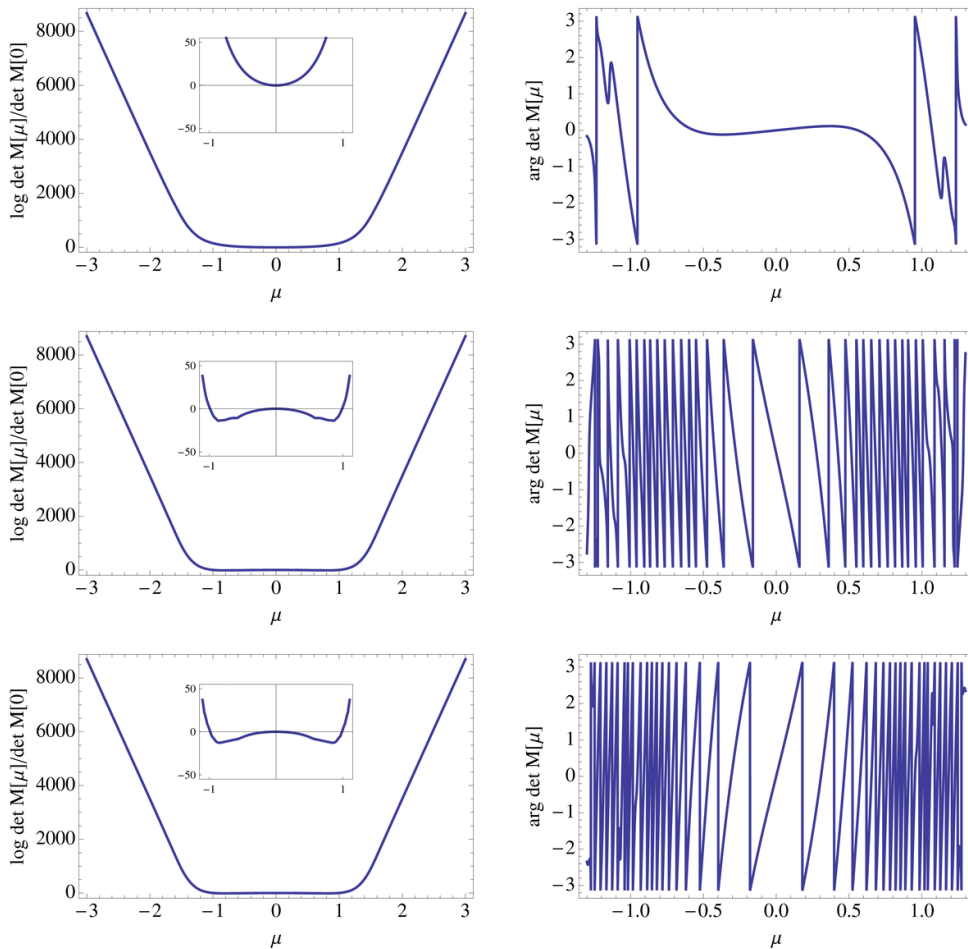


Figure 3: The logarithm of the determinant $|\det M(\mu)|$ normalised to $\det M(\mu = 0)$ (left row) and the argument of $\det M(\mu)$ (right row) for three configurations from a canonical ensemble with $n_B = 4$. From top to bottom the configurations have $\arg P(U) \approx 0, +2\pi/3$ and $-2\pi/3$.

same one used in the middle panel of figure 4). We see that the magnitude now increases monotonically and that the phase changes much slower with μ – this is exactly the behavior of configurations that have $\arg P(U) \approx 0$.

As we emphasized in the introduction these observations are hard to interpret physically, but we believe that they might play an important role for the optimization of reweighting strategies, or for the development of new canonical simulation algorithms.

5.2 Calculation of the projected determinants

Using eq.(43) we can show that the projected determinants $\det_k M$ defined in eq.(3), up to a multiplication with $\det Q$, are the coefficients $c_{k+k_{\max}}$ of the polynomial

$$\Pi(x) = \prod_{i=1}^{2k_{\max}} (x + \lambda_i) = \sum_{k=0}^{2k_{\max}} c_k x^k, \quad (46)$$

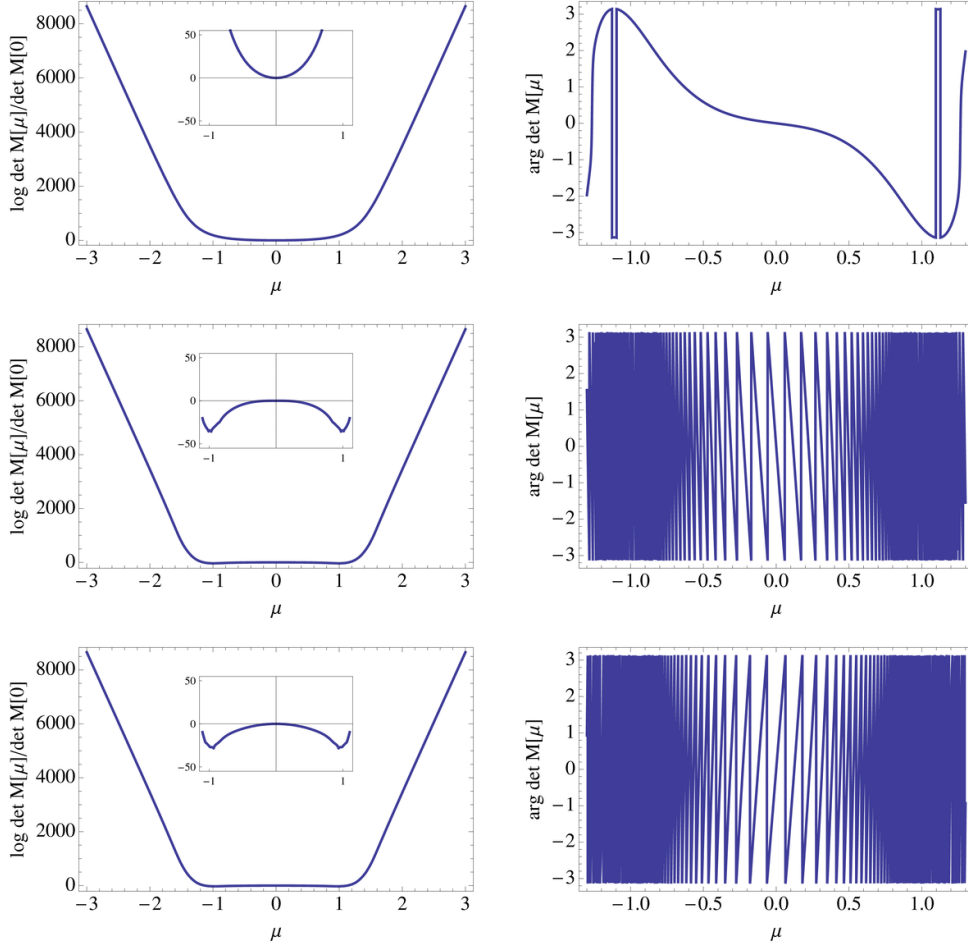


Figure 4: Same as Fig. 3, but for three configurations from a canonical ensemble with $n_B = 11$.

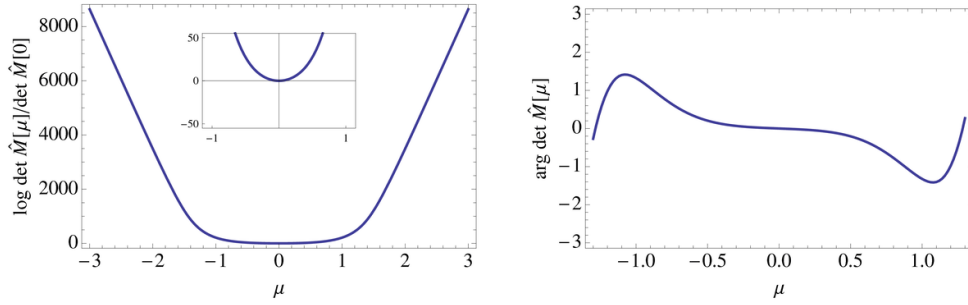


Figure 5: Same as the middle panel of Fig. 4 but for the modified determinant eq.(45).

where $k_{\max} = 2N_c N_s^3$. A couple of coefficients can be computed easily: $c_{2k_{\max}} = 1$ and $c_0 = \prod_i \lambda_i = \det T \cdot \mathcal{U} = 1$ as discussed before. All other coefficients can be calculated recursively. To show this, we first define the partial product:

$$\Pi_n(x) = \prod_{i \leq n} (x + \lambda_i) = \sum_{k \leq n} c_k^{(n)} x^k. \quad (47)$$

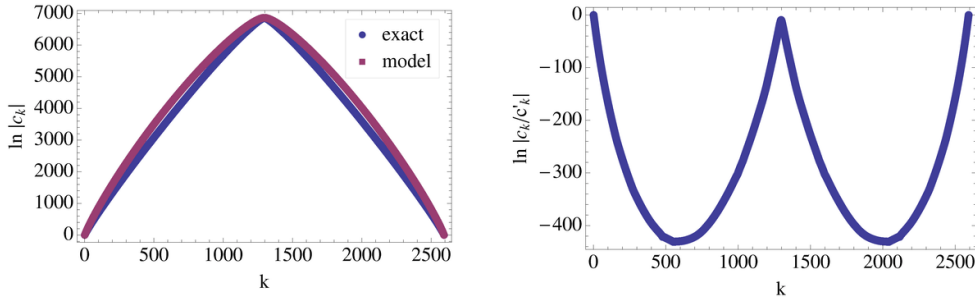


Figure 6: Simple model calculation: on the left the exact values and the model values are shown. In the right panel the ratio between the exact and model values are shown.

Clearly, $\Pi_{n+1}(x) = (x + \lambda_{n+1})\Pi_n(x)$ and hence we have

$$c_k^{(n+1)} = \lambda_{n+1}c_k^{(n)} + c_{k-1}^{(n)}, \quad (48)$$

for all $0 \leq k \leq n+1$ (we set $c_{-1}^{(n)} = 0$). For Π_0 all coefficients are zero except for $c_0^{(0)} = 1$. Using eq.(48) to compute $c_k^{(n+1)}$ from $c_k^{(n)}$, after $2k_{\max}$ steps we obtain the coefficients of $\Pi_{2k_{\max}} \equiv \Pi$.

The recursive steps of the iteration have to be carried out using a high precision library. The reason for this is that the magnitude of the coefficients vary over thousands of orders of magnitude. We used GNU Multi-Precision library which can easily handle numbers of this magnitude. While the calculation takes significantly longer than when using the standard floating point arithmetic, the total time is small compared to the time it takes to compute the eigenvalues of the reduced matrix. One possible issue when using a high precision library is that the results look deceptively precise since the inputs are treated as high precision numbers when their real precision is at the level of machine precision or less. To check the robustness of our calculation we performed the following tests. In the first test we added random numbers of the order of 10^{-15} (double precision level) to the links and recomputed the projected determinants; the relative change in the projected determinants was at the level of 10^{-10} . Next, we randomly reordered the eigenvalues of the reduced matrix and repeated the recursive step. We find that the relative change in the coefficients is of the order of 10^{-9} . We conclude that our procedure is robust and it produces accurate results.

Before we conclude this section, we want to point out that the $\lambda \leftrightarrow 1/\lambda^*$ symmetry of the reduced matrix, together with the fact that $\det T \cdot \mathcal{U} = 1$ can be used to show that $c_{k_{\max}+k} = c_{k_{\max}-k}^*$. Since $\det \mathcal{Q}$ is real, this insures that that $\det_k M = (\det_{-k} M)^*$ a fact easily derived from the definition of the projected determinant and the reality of $\det M(\phi)$.

5.3 Size distribution of the projected determinant

One of the interesting aspects of this calculation is the fact that the magnitude of the projected determinants varies over many orders of magnitude as we change the quark number sector. In this section we will show that the bulk of this variance can be captured by a simple combinatorial argument. However, this only captures part of the variance: in order to describe the variance accurately we need to take into account the complex phase of the eigenvalues of the reduced matrix.

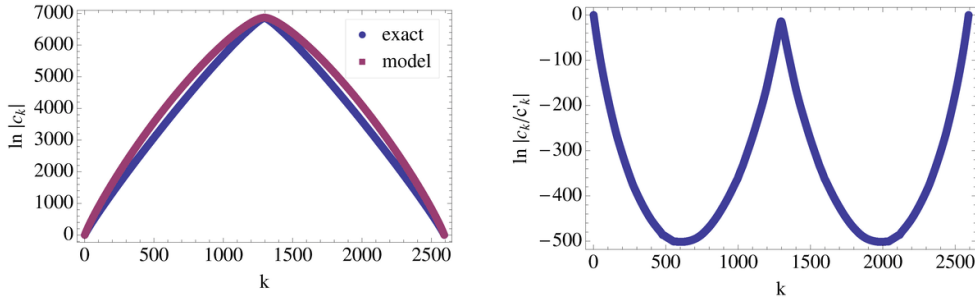


Figure 7: Comparison between true polynomial coefficients and the ones where the eigenvalue phase is quenched.

In the main, the bulk of the magnitude is given by the average magnitude of the eigenvalues and combinatorics. To illustrate this point, in Fig. 6 we compare the value of the coefficients of the polynomial $\Pi(x)$ for a given configuration with the coefficients of the polynomial $\Pi'(x) = (x + \bar{\lambda})^{k_{\max}}(x + 1/\bar{\lambda})^{k_{\max}}$, where $\bar{\lambda}$ is the geometric mean of the magnitude of the large eigenvalues $\bar{\lambda} = \left(\prod_{|\lambda|>1} |\lambda_i|\right)^{1/k_{\max}}$.

For any given configurations the eigenvalues vary both in phase and magnitude; in the comparison above we quenched both fluctuations. While this approximation captures a good part of the variation of magnitude, there is still quite a discrepancy left. To trace the source of discrepancy we compare the coefficients of $\Pi(x)$ with a polynomial where each eigenvalue is replaced with its magnitude: $\Pi''(x) = \prod_i (x + |\lambda_i|)$. The results of this comparison are presented in Fig. 7: we see that the discrepancy is similar to the one above. This shows that the source of discrepancy is the complex phase fluctuation that is disregarded here. This conclusion is also supported by the fact that the coefficients of $\Pi''(x)$ are larger in magnitude than the coefficients of $\Pi(x)$; this is due to cancellations produced by phase fluctuations.

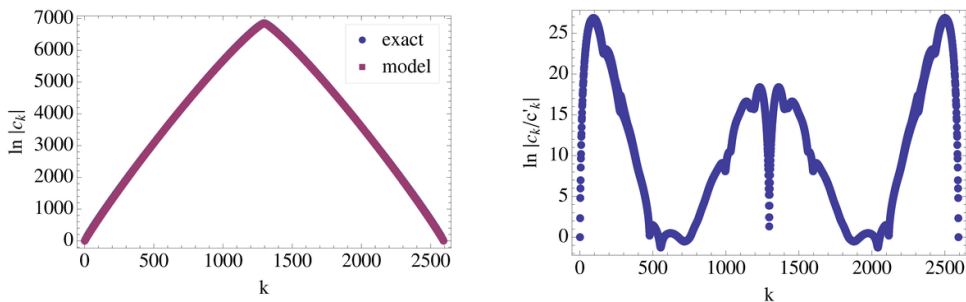


Figure 8: Comparison between true polynomial coefficients and the ones where the eigenvalue phase is drawn from a random $\mathbb{Z}(3)$ distribution. Note the difference in scale in the right plot as compared to Fig. 7 and 6.

To prove that phase fluctuations are responsible for the discrepancy we model the rough features of the phase distribution. The phase distribution is illustrated in Fig. 1. One obvious feature is that the eigenvalues are concentrated around the $\mathbb{Z}(3)$ axes. This makes sense: if the eigenvalues were exactly along the $\mathbb{Z}(3)$ axes, the projected determinants that have zero triality ($k = 3n_B$) will be real whereas the ones with non-zero triality will have a fluctuating phase and they will vanish when averaged over gauge configurations, as expected.

To check that phase fluctuations are responsible for reducing the magnitude of the coefficients we compare the coefficients of $\Pi(x)$ with $\Pi'''(x) = \prod_i (x + z_i |\lambda_i|)$, where z_i is a random $\mathbb{Z}(3)$ phase with one constraint: we enforce the $(\lambda, 1/\lambda^*)$ pairing. The results are presented in figure 8: we see that the results agree much better now. It is clear that the phase fluctuations play an important role in determining the coefficients. Phase fluctuations reduce the value of the coefficients significantly: from figure 7 we see that for intermediate k values they reduce the magnitude by about 200 orders of magnitude. From figure 8 we see that this is mostly due to the $\mathbb{Z}(3)$ nature of the fluctuations (we also tested random $\mathbb{Z}(n)$ phases with $n \in \{2, 4, 5, 6\}$ but they fail to produce the same agreement).

6 Phase fluctuations in canonical ensembles

The reduced Wilson fermion matrix constructed and discussed in the previous sections allows for several intriguing applications. Presumably among the most interesting are the direct simulation of canonical ensembles and the reweighting to different fermion numbers, or values of the chemical potential. In the following we briefly discuss these two applications and present some results on the phase fluctuations encountered in direct simulations of canonical ensembles, merely to illustrate the capabilities of the reduced fermion matrix approach.

In order to simulate the canonical partition function eq.(2) by Monte-Carlo techniques one needs the integrand to be real and positive. Since in general this is not guaranteed, the approach so far [7] has been to ensure positivity by fiat, i.e. to generate an ensemble using the weight $W_{|k|}(U) \propto |\text{Re det}_k M(U)|$, while the phase

$$\alpha(U) \equiv \frac{\det_k M(U)}{W_{|k|}(U)} \quad (49)$$

is introduced when computing the observable

$$\langle O(U) \rangle_k = \frac{\langle O(U) \alpha(U) \rangle_{|k|}}{\langle \alpha(U) \rangle_{|k|}}, \quad (50)$$

where $\langle \cdot \rangle_{|k|}$ denotes the average with regard to the generated ensemble based on the $W_{|k|}$ measure. In practice, to evaluate the partition function numerically, the continuous Fourier transform in eq.(3) has so far either been replaced by a discrete Fourier transform [7] or by a more sophisticated approximation [27, 25] and the so introduced bias needs a careful treatment. With the reduced Wilson fermion matrix these approximations have become obsolete, simply because the Fourier transform can now be evaluated exactly.

Still, the quenching of the phase of the integration measure, $\det_k M(U) \rightarrow W_{|k|}$, introduces a systematic error which one needs to control. A measure of how severe the fluctuations of the phase are, is provided by the expectation value of $\alpha(U)$ in eq.(49) in a given ensemble. It turns out that the sign fluctuations for the canonical ensembles seem to be under good control and one might wonder how generic this feature is. One way to estimate the reliability of the simulations is to reweigh results generated at one value of k to other values k' and to check consistency between the reweighted results and the ones obtained from direct simulations. For the reweighting from one canonical ensemble $Z_C(k)$ to another $Z_C(k')$ the relevant quantity is

$$\alpha_{|k| \rightarrow k'}(U) = \frac{\det_{k'} M(U)}{W_{|k|}(U)}. \quad (51)$$

For this definition of the reweighting factor we see from the second column of Table 1 that its magnitude changes very fast as we move away from the original ensemble, in this case the one with $n_B = 4$. However, the value of the factor changes for all configurations in a similar manner and the average is still comfortably away from zero in terms of its variance (cf. third and fourth column) even though its magnitude is dramatically changed. (Note that this dramatic change is related to the variation of $\det_k M$ with k over many orders of magnitude.) What we mean by that is that its magnitude, as compared with its variance, is larger than two or more. In principle it is when this ratio becomes close to one that the reweighting in the equation above will run into numerical difficulties. We see from Table 1 that for baryon numbers as large as $n'_B = 16$ the average is still twice the variance.

| n_B | $\langle \alpha \rangle$ | σ_α | $\sigma_\alpha / \langle \alpha \rangle$ |
|-------|--------------------------|-----------------------|--|
| 00 | $7.63 \cdot 10^{+2}$ | $3.93 \cdot 10^{+2}$ | 0.515 |
| 04* | $4.87 \cdot 10^{-1}$ | $3.09 \cdot 10^{-2}$ | 0.064 |
| 08 | $1.60 \cdot 10^{-4}$ | $1.21 \cdot 10^{-5}$ | 0.076 |
| 12 | $7.78 \cdot 10^{-9}$ | $1.11 \cdot 10^{-9}$ | 0.143 |
| 16 | $1.82 \cdot 10^{-14}$ | $9.81 \cdot 10^{-15}$ | 0.540 |

Table 1: The real part of the average reweighting factor eq.(51). The imaginary part vanishes by symmetry. This factor is computed based on the ensemble generated with $n_B = 4$ (marked with a star above).

In Fig. 9 we plot the ratio between the variance and the average of the real phase factor reweighted from the canonical ensembles with $n_B = 4$ and 11, as a function of the reweighted baryon number. Note that in both cases the average reweighting factor is well behaved over a large range of reweighted baryon numbers.

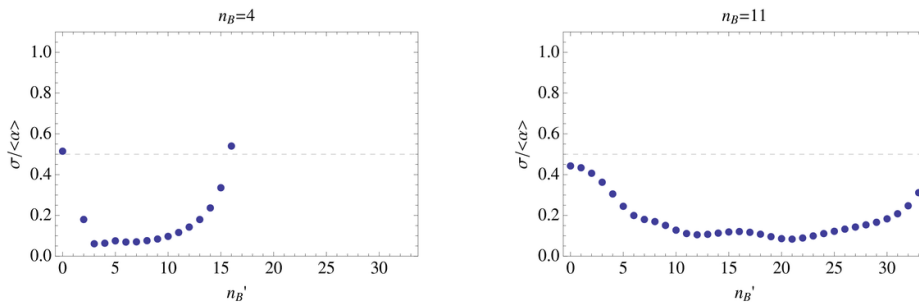


Figure 9: The real part of the average phase factor: the ratio between its variance and its mean value.

Encouraged by this result one might also try to reweight the chemical potential as a function of the baryon number following the definition in eq.(5). The chemical potential, as defined there, can be shown to be

$$\mu_B(n_B)/T = -\log \frac{Z_C(3(n_B + 1))}{Z_C(3n_B)} = -\log \left\langle \frac{\det_{3(n_B+1)} M}{\det_{3n_B} M} \right\rangle_{3n_B} \quad (52)$$

$$= -\log \frac{\langle \det_{3(n_B+1)} M / W_{|3n_B|} \rangle_{|3n_B|}}{\langle \det_{3n_B} M / W_{|3n_B|} \rangle_{|3n_B|}}. \quad (53)$$

In Fig. 10 we show the reweighted chemical potential as defined by eq.(5), for the same ensembles as before, $n_B = 4$ (left plot) and $n_B = 11$ (right plot). Despite the absence of a sign problem in the reweighting factor, it is evident that the reweighting fails. The ensemble $n_B = 4$ in the confined phase misses to describe even the neighbouring ensemble with only slightly different baryon number $n_B = 5$. The ensemble $n_B = 11$, on the other hand, is in the deconfined phase and seems to be able to describe other deconfined phases with different baryon numbers. Not surprisingly, however, it completely fails to describe ensembles with $n_B \leq 8$, and hence the phase transition, simply because it does not contain any information about the confined phase.

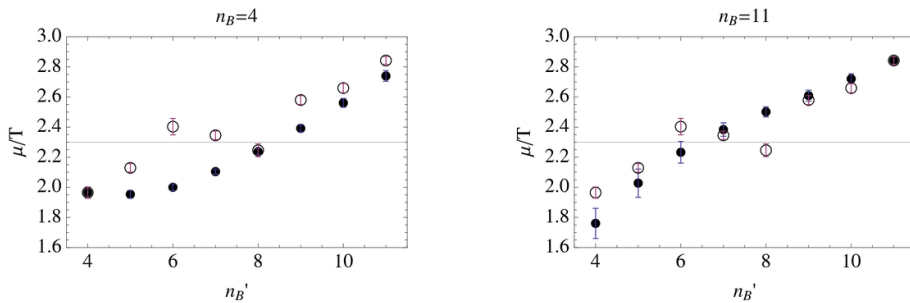


Figure 10: The baryon chemical potential reweighted from the ensemble with $n_B = 4$ (left plot) and $n_B = 11$ (right plot). Empty circles are the results of the direct calculation.

The next interesting question would now be to reweight an ensemble in the mixed phase, e.g. with $n_B = 7$. However, the reweighted results turn out to be too noisy, indicating that the information gathered in the canonical ensembles is simply not enough to allow for a reliable reweighting. One has to keep in mind that the canonical ensembles used here only contain about 1500 configurations each. The next obvious step is then to employ a multi-ensemble reweighting, combining the information from all the ensembles into the reweighting. What we find is that for $n_B' = 4$ the most important contributions indeed come from the ensembles with small n_B and that, as we move towards larger n_B' , higher ensembles come into play as expected. However, even the multi-ensemble reweighting does not seem capable to reproduce the S-shape behaviour typical for a first order phase transition, and we conclude that the reweighting suffers from a severe overlap problem. Nevertheless, the example impressively demonstrates the ease with which such calculations can be achieved using the reduced Wilson fermion matrix.

7 Conclusions

We have presented a reduction method for Wilson Dirac fermions which generates a dimensionally reduced fermion matrix. The size of the reduced matrix is independent of the temporal lattice extent. Moreover, the dependence of the matrix on the chemical potential factors out and reduces to a simple multiplicative factor. This allows to evaluate the Wilson fermion determinant for any value of the chemical potential, once the eigenvalues of the reduced matrix are calculated, and hence allows to perform the exact projection of the determinant to the canonical sectors with fixed fermion number.

The reduced fermion matrix presented here facilitates various interesting applications, for example the reweighting of ensembles to arbitrary values of the chemical potential or the fermion number. So far, this has only been possible for staggered fermions. Another application is the direct simulation of canonical ensembles and this is now possible without any bias from inexact projections to the canonical sectors. Since the size of the reduced matrix is independent of the temporal lattice extent, such calculations can in principle be done at arbitrarily low temperatures, barring possible sign problems.

The reduced fermion matrix has some interesting properties like the spectral symmetry $\lambda \leftrightarrow 1/\lambda^*$, a simple behavior of the spectrum under $\mathbb{Z}(N_c)$ -transformations and the correlation of the spectrum with the Polyakov loop. We believe that such properties may be important for the development of more efficient canonical simulation algorithms, or for the optimisation of reweighting strategies.

As a first test we applied the reduction method to a set of canonical ensembles and determined the phase fluctuations of the Wilson fermion determinant at non-zero chemical potential, or non-zero fermion number, using standard reweighting techniques. It turns out that for the ensembles considered here, the overlap problem inherent in all reweighting methods introduces a systematic bias that forbids reliable calculations, e.g. using multi-ensemble reweighting. On the other hand, the phase fluctuations seem to be rather well controlled and it will be interesting to see whether this is a generic feature of canonical partition functions.

Acknowledgements

We would like to thank Philippe de Forcrand for discussions, and Atsushi Nakamura and Keitaro Nagata for correspondence on their related work. Andrei Alexandru is supported in part by U.S. Department of Energy under grant DE-FG02-95ER-40907. The computational resources for this project were provided by the George Washington University IMPACT initiative. We would like to thank Anyi Li for providing us with the configurations needed for this study.

References

- [1] P. E. Gibbs, *The fermion propagator matrix in lattice QCD*, *Phys. Lett.* **B172** (1986) 53.
- [2] I. M. Barbour, C. T. H. Davies, and Z. Sabeur, *Lattice QCD at finite density*, *Phys. Lett.* **B215** (1988) 567–572.
- [3] A. Hasenfratz and D. Toussaint, *Canonical ensembles and nonzero density quantum chromodynamics*, *Nucl. Phys.* **B371** (1992) 539–549.
- [4] J. Danzer and C. Gattringer, *Winding expansion techniques for lattice QCD with chemical potential*, *Phys. Rev.* **D78** (2008) 114506, [[arXiv:0809.2736](https://arxiv.org/abs/0809.2736)].
- [5] C. Gattringer and L. Liptak, *Canonical fermion determinants in lattice QCD - Numerical evaluation and properties*, [arXiv:0906.1088](https://arxiv.org/abs/0906.1088).

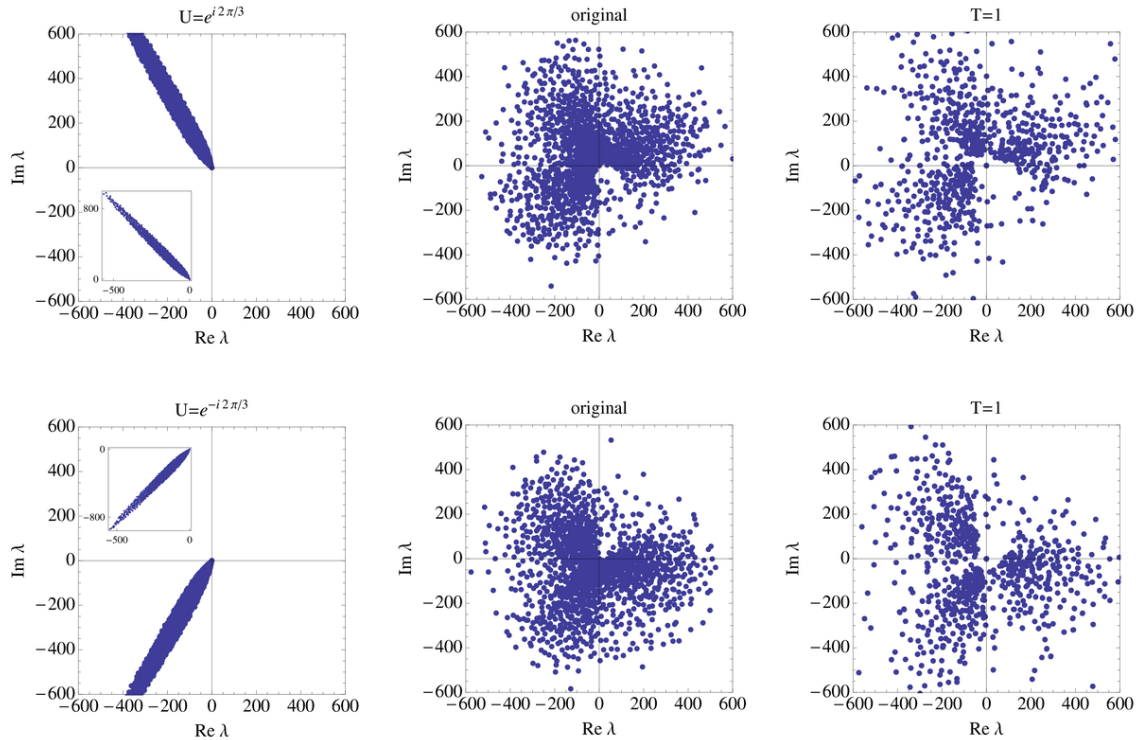


Figure 11: Same as figure 2, but for a configuration with $\arg P(U) \approx +2\pi/3$ (top row) and one with $\arg P(U) \approx -2\pi/3$.

- [6] S. Kratochvila and P. de Forcrand, *The canonical approach to finite density QCD*, *PoS LAT2005* (2006) 167, [[hep-lat/0509143](#)].
- [7] A. Alexandru, M. Faber, I. Horvath, and K.-F. Liu, *Lattice QCD at finite density via a new canonical approach*, *Phys. Rev.* **D72** (2005) 114513, [[hep-lat/0507020](#)].
- [8] Z. Fodor, K. K. Szabo, and B. C. Toth, *Hadron spectroscopy from canonical partition functions*, *JHEP* **08** (2007) 092, [[arXiv:0704.2382](#)].
- [9] P. de Forcrand, M. A. Stephanov, and U. Wenger, *On the phase diagram of QCD at finite isospin density*, *PoS LAT2007* (2007) 237, [[arXiv:0711.0023](#)].
- [10] A. Borici, *Computational methods for the fermion determinant and the link between overlap and domain wall fermions*, [[hep-lat/0402035](#)].
- [11] R. G. Edwards, B. Joo, A. D. Kennedy, K. Orginos, and U. Wenger, *Comparison of chiral fermion methods*, *PoS LAT2005* (2006) 146, [[hep-lat/0510086](#)].
- [12] R. G. Edwards, B. Joo, A. D. Kennedy, K. Orginos, and U. Wenger, *Five dimensional variants of overlap fermions*, *in preparation*.
- [13] A. Borici, *Reweighting with stochastic determinants*, *Prog. Theor. Phys. Suppl.* **153** (2004) 335–339.

- [14] A. Nakamura and K. Nagata, *private communication*.
- [15] Z. Fodor and S. D. Katz, *A new method to study lattice QCD at finite temperature and chemical potential*, *Phys. Lett.* **B534** (2002) 87–92, [[hep-lat/0104001](#)].
- [16] C. R. Allton *et. al.*, *The QCD thermal phase transition in the presence of a small chemical potential*, *Phys. Rev.* **D66** (2002) 074507, [[hep-lat/0204010](#)].
- [17] P. de Forcrand and O. Philipsen, *The QCD phase diagram for small densities from imaginary chemical potential*, *Nucl. Phys.* **B642** (2002) 290–306, [[hep-lat/0205016](#)].
- [18] M. D’Elia and M.-P. Lombardo, *Finite density QCD via imaginary chemical potential*, *Phys. Rev.* **D67** (2003) 014505, [[hep-lat/0209146](#)].
- [19] S. Kratochvila and P. de Forcrand, *QCD at small baryon number*, *Nucl. Phys. Proc. Suppl.* **140** (2005) 514–516, [[hep-lat/0409072](#)].
- [20] A. Alexandru, M. Faber, I. Horvath, and K.-F. Liu, *Progress on a canonical finite density algorithm*, *Nucl. Phys. Proc. Suppl.* **140** (2005) 517–522, [[hep-lat/0410002](#)].
- [21] S. Ejiri, *Canonical partition function and finite density phase transition in lattice QCD*, *Phys. Rev.* **D78** (2008) 074507, [[arXiv:0804.3227](#)].
- [22] A. Roberge and N. Weiss, *Gauge theories with imaginary chemical potential and the phases of QCD*, *Nucl. Phys.* **B275** (1986) 734.
- [23] S. Kratochvila and P. de Forcrand, *QCD at zero baryon density and the Polyakov loop paradox*, *Phys. Rev.* **D73** (2006) 114512, [[hep-lat/0602005](#)].
- [24] P. Hasenfratz and F. Karsch, *Chemical Potential on the Lattice*, *Phys. Lett.* **B125** (1983) 308.
- [25] A. Li, A. Alexandru, K.-F. Liu, and X. Meng, *Finite density phase transition of QCD with $N_f = 4$ and $N_f = 2$ using canonical ensemble method*, [[arXiv:1005.4158](#)].
- [26] P. de Forcrand and V. Laliena, *The role of the Polyakov loop in finite density QCD*, *Phys. Rev.* **D61** (2000) 034502, [[hep-lat/9907004](#)].
- [27] X.-f. Meng, A. Li, A. Alexandru, and K.-F. Liu, *Winding number expansion for the canonical approach to finite density simulations*, *PoS LATTICE2008* (2008) 032, [[arXiv:0811.2112](#)].